Journal of Power Sources 257 (2014) 90–95

Contents lists available at ScienceDirect

Journal of Power Sources

journal homepage: www.elsevier.com/locate/jpowsour

CuInZnS-decorated graphene as a high-rate durable anode for lit© 2014 Elsevier B.V. All rights reserved.hium-ion batteries

Xiaosheng Tang [a,b], Xiayin Yao [a], Yu Chen [c], Bohang Song [d], Dan Zhou [a], Junhua Kong [a], Chenyang Zhao [a], Xuehong Lu [a,*]

[a] School of Materials Science & Engineering, Nanyang Technological University, Singapore 639798, Singapore
[b] College of Optoelectronic Engineering, Chongqing University, Chongqing 400044, PR China
[c] Department of Materials Science & Engineering, National University of Singapore, Singapore 117574, Singapore
[d] Department of Mechanical Engineering, National University of Singapore, Singapore 117574, Singapore

HIGHLIGHTS

- CuInZnS-decorated graphene nanosheets were used as LIB anode materials for the first time.
- It was demonstrated that CuInZnS has multiple alloying reactions with lithium ions.
- The CuInZnS-decorated graphene anode showed enhanced rate capability and cycling stability.

GRAPHICAL ABSTRACT

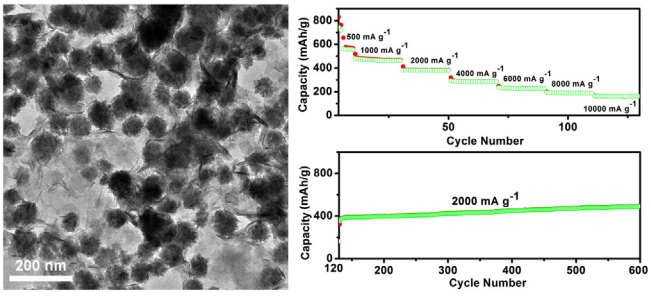

ARTICLE INFO

Article history:
Received 21 December 2013
Received in revised form
23 January 2014
Accepted 25 January 2014
Available online 1 February 2014

Keywords:
Quaternary sulfide
Graphene
Hydrothermal
Rate capability
Lithium-ion battery

ABSTRACT

CuInZnS-decorated graphene (CIZS@graphene) is prepared *via* a hydrothermal process and investigated as an anode material for lithium-ion batteries. CIZS@graphene exhibits an initial discharge capacity of 1623 mA.h g^{-1} at 100 mA g^{-1}, and at a high rate of 2000 mA g^{-1} its reversible capacity is steadily increased from 389 mA h g^{-1} to 494 mA h g^{-1} in 480 cycles, demonstrating promising stable cycling performance at high rates. Electrochemical impedance spectroscopic studies show that charge-transfer resistances of CIZS@graphene reduces after cycling at high rates, justifying the excellent high-rate performance and stability of the CIZS@graphene anode.

1. Introduction

Rechargeable lithium-ion batteries (LIBs) have attracted much attention recently and been considered as one of the most promising candidates for energy storage owing to their light weight, high energy density, and strong potentials for emerging applications such as various portable electronic devices and electrical/hybrid vehicles [1–7]. As a commercial anode material in LIBs, graphite has advantages including high electrical conductivity, good structural stability during cycling and hence long cycle life. However, it has relatively low theoretic capacity of only 372 mA h g^{-1} [8–10]. In addition, the slow kinetics of lithium ion diffusion in graphite affects high-rate charge–discharge performance. In order to meet the

* Corresponding author. Tel.: +65 6790 4585; fax: +65 6790 9081.
E-mail address: asxhlu@ntu.edu.sg (X. Lu).

0378-7753/$ – see front matter © 2014 Elsevier B.V. All rights reserved.
http://dx.doi.org/10.1016/j.jpowsour.2014.01.107

requirements for many emerging technologies, the next generation of LIB anodes must have superior performance including much enhanced capacity, rate performance and cycling stability.

Transition metal oxides have been widely studied as anode materials for LIBs as alternatives to graphite. These compounds in general exhibit higher capacities than that of graphite due to their redox and Li-alloying reactions. More recently, binary metallic sulfides, such as CuS [11], ZnS [12] and FeS_2 [13], have also been explored as anode materials for LIBs. However, these sulfides suffer from serious irreversible capacity decay after the first cycle, restraining their applications in LIBs. In contrast to the sulfides mentioned above, indium sulfide (In_2S_3) [14–16], a typical III–VI group sulfide, is able to alloy with lithium more reversibly, forming Li_xIn where x may vary from 0 to 4.33 depending on the alloying configuration. The maximum theoretical irreversible and reversible capacities of In_2S_3 are estimated to be *ca.* 494 mA h g^{-1} and *ca.* 713 mA h g^{-1}, respectively, which are much higher than that of graphite [14–16]. Moreover, it is generally recognized that the introduction of Cu or Zn into a metallic sulfide would greatly improve the electrical conductivity of the host material and hence benefit the reversible capacity of the material [17]. For example, Wang and coworkers reported that mesoporous Cu_2SnS_3 spheres exhibited a high initial capacity of 891 mA h g^{-1} and stable reversible capacity during subsequent cycles [18]. Thus, Cu- and Zn-doped indium sulfide alloy nanomaterials may be promising high-performance anode materials for LIBs. Since CuInZnS (CIZS) contains not only a transition metal Cu but also two Li-alloyable elements, In and Zn, multiple alloying reactions and hence a high capacity could be expected from this material [17,19,20]. However, although CIZS nanomaterials have been shown to have promising photocatalytic activity for hydrogen evolution under visible light irradiation [19,21,22], to the best of knowledge, the application of the quaternary CIZS as an anode material in LIBs has not been reported.

Very recently, graphene-based nanocomposites have also attracted great attention for LIB applications due to their excellent electrical conductivity, mechanical property and chemical stability. In particular, the extremely large surface area and porosity of nanoparticle-decorated graphene nanosheets may greatly benefit high-rate performance and stability of the LIB electrodes. Graphene-based Fe_3O_4 [10,23,24], Co_3O_4 [25] and MnO_2 [26] nanocomposites have been shown to exhibit excellent electrochemical properties as LIB anodes. Jiang's group reported that the LIB anodes based on graphene–In_2S_3 nanocomposites also exhibited higher specific capacities than neat In_2S_3 [14,16].

In this work, to utilize the potential high reversible capacity of CIZS and excellent properties of graphene, CuInZnS-decorated graphene nanosheets (CIZS@graphene) were investigated as an LIB anode material for the first time. Herein, we report the excellent electrochemical performance of the CIZS@graphene anode. Our results show that the CIZS@graphene anode exhibits an initial discharge capacity of 1623 mA h g^{-1} at 100 mA g^{-1} and a stabilized value of about 494 mA h g^{-1} after 480 cycles at a high current rate of 2000 mA g^{-1}. Such greatly improved rate capacity and stability demonstrate significant advantages of CIZS@graphene for LIB applications. To illustrate the mechanisms underlying the excellent rate capacity and stability of CIZS@graphene, electrochemical impedance spectroscopic (EIS) studies were also conducted to probe the synergistic effects between CIZS and graphene.

2. Experimental

2.1. Preparation of CIZS and reduced graphene oxide (rGO)

CIZS was prepared *via* a hydrothermal method [22]. In a typical experiment, $Zn(Ac)_2{\cdot}2H_2O$ (219 mg), $InCl_3{\cdot}4H_2O$ (65.89 mg), CuCl (2.4 mg), and excess amount of thioacetamide (200 mg) were dissolved into 15 mL of distilled water using a magnetic stirrer to form a clear solution. The reaction mixture was immediately transferred into an autoclave (Teflon cups with 50 mL inner volume). The autoclave was maintained at 180 °C for 18 h and then air-cooled to room temperature. The product was collected by centrifugation, washed several times with absolute ethanol and finally air dried. Graphene oxide (GO) was prepared by oxidation of natural flake graphite powder using a modified Hummers method, and reduced by Zinc powder [27].

2.2. Preparation of CIZS@graphene

In a typical synthesis process, the as-prepared rGO and the precursor including $Zn(Ac)_2{\cdot}2H_2O$ (219 mg), $InCl_3{\cdot}4H_2O$ (65.89 mg), CuCl (2.4 mg) and excessive thioacetamide (200 mg) were mixed in 15 mL distilled water. The mixture was sonicated for 30 min. The mixture was then immediately transferred into an autoclave (Teflon cups with 50 mL inner volume). The autoclave was maintained at 180 °C for 18 h and then air-cooled to room temperature. The product was collected by centrifugation and washed several times with absolute ethanol and finally dried in air. The weight ratio of graphene to CIZS was about 5:95 based on the feed ratio.

2.3. Characterization

The morphology of CIZS@graphene was examined using a field-emission scanning electron microscope (FESEM; XL 30 FEG Philips, Hillsboro, OR). Samples were prepared by dipping carbon-coated copper grids into the sample solution followed by drying at room temperature. All transmission electron microscopy (TEM) images were obtained using a JEOL 3010 microscope at an acceleration voltage of 200 kV. Crystal structures of the materials were investigated using an Advanced Diffractometer System (D8 Advanced Diffractometer System, Bruker, Karlsruhe, Germany). Brunauer–Emmett–Teller (BET) specific surface areas and pore volumes were calculated from nitrogen adsorption/desorption isotherms determined at 77 K using an AUTO-SORB-1-MP surface analyzer (the sample was outgassed under vacuum at 200 °C).

2.4. Electrochemical measurements

To prepare working electrodes, an active material (CIZS nanospheres or CIZS@graphene), carbon black (super P) and poly(-vinylidene fluoride) were firstly mixed in the weight ratio of 80:10:10 in *n*-methyl-2-pyrrolidone. The slurries were stirred overnight to achieve uniform dispersion. Then the slurry was pasted onto a copper foil with radius controlled in the range of 7–8 mm to form a working electrode. Before assembling the batteries, the working electrodes were dried in a vacuum oven at 120 °C for at least 12 h. For galvanic charge and discharge testing, a half-battery cell was assembled using the aforementioned electrode as the anode, pure Li foil as the counter electrode, two pieces of Celgard 2500 membranes as separators, and 6-10 drops of 1 M $LiPF_6$ in organic solutions of EC:DEC:DMC (weight ratio = 1:1:1) as the electrolyte. Swagelok mound was applied for half-battery assembly in an argon-filled glove-box. All the tests were conducted in a voltage range of 0.05–3.0 V versus Li^+/Li^0 at room temperature. The cyclic voltammetry (CV) test was performed on an electrochemical workstation (PGSTAT302, Autolab) with a voltage window of 3.0–0.05 V and at a scan rate of 0.1 mV s^{-1}. EIS study was conducted using the same electrochemical workstation in a frequency range of 10^5–10^{-2} Hz and at the a.c. amplitude of 5 mV.

3. Results and discussion

Fig. 1A shows an FESEM image of the as-prepared CIZS@-graphene which contains 95 wt% CIZS. The atomic ratio of the CIZS is $Cu_{0.02}In_{0.3}ZnS_{1.47}$ [19,22]. It is observed that CIZS nanoparticles are firmly attached on graphene sheets, which may act as conducting medium to ensure smooth lithium insertion/extraction into/from the CIZS nanoparticles because of the high electrical conductivity of graphene. TEM studies reveal that the CIZS nanoparticles on graphene nanosheets are spherical in shape and the average size of the nanospheres is around 80 nm (Fig. 1B), which is slightly smaller than that of neat CIZS nanospheres (100 nm; Fig. S1). Energy dispersive X-ray spectrum (EDS) of CIZS@graphene (Fig. S2) shows that Cu, In, Zn and S are the major elements of the nanocomposite. X-ray energy dispersive spectrometry (XEDS) was carried out on the same nanosphere in scanning transmission electron microscopy (STEM) mode (Fig. S3). The XEDS studies confirmed the homogeneous distribution of Cu, In and Zn elements throughout the nanosphere, suggesting that the CIZS alloy has a single-phase structure. Similar to the neat CIZS nanospheres, the nanospheres attached on graphene are also composed of very small nanoparticles. The high-resolution TEM image in Fig. 1C shows lattice fringes of the nanoparticles in the nanospheres, indicating that the nanoparticles are highly crystalline. The lattice spacing was measured to be around 0.31 nm, which could be assigned to the (111) plane of CIZS crystal structure. Fig. 1D shows the X-ray diffraction (XRD) patterns of the neat CIZS nanospheres and CIZS@graphene. The main diffraction peaks of both samples are at $2\theta = 28.6^\circ$, 47.6° and 56.5°, which are corresponding to the diffraction from the (111), (220) and (311) planes of ZnS and hence can be indexed to ZnS (JCPDS No. 65-0309). This confirms the cubic zinc blende structure of the CIZS nanospheres [19,22]. In general all diffraction peaks are broad because the nanospheres are composed of smaller nanoparticles with very small crystal size. It is, however, worth noting that the diffraction peaks from the neat CIZS nanospheres are slightly sharper than that of CIZS@graphene, indicating that the crystals in CIZS@graphene are smaller than that in the neat CIZS nanospheres. From the XRD patterns, the characteristic diffraction peaks for graphene are not observed because the low content and low diffraction intensity of graphene.

BET gas-sorption measurement results show that mesopores are present in both the neat CIZS nanospheres (Fig. S3) and CIZS@-graphene (Fig. 2). The specific surface area of CIZS@graphene is 120.5 $m^2\ g^{-1}$, which is much higher than that of the neat CIZS nanospheres (81.84 $m^2\ g^{-1}$) owing to the much lower density of rGO and probably also the smaller nanosphere and crystal sizes in CIZS@graphene. The larger surface area of CIZS@graphene is beneficial for the electrolyte diffusion to active sites. Moreover, the high porosity of CIZS@graphene implies that the volume change of CIZS during Li-ion insertion/removal may be well accommodated, which may help in retaining the structural integrity and the overall capacity of the anode during cycling. Therefore, promising capacity retention property is expected from CIZS@graphene anode material.

The electrochemical properties of the CIZS nanosphere and CIZS@graphene based anodes were investigated in a CR2016 coin-

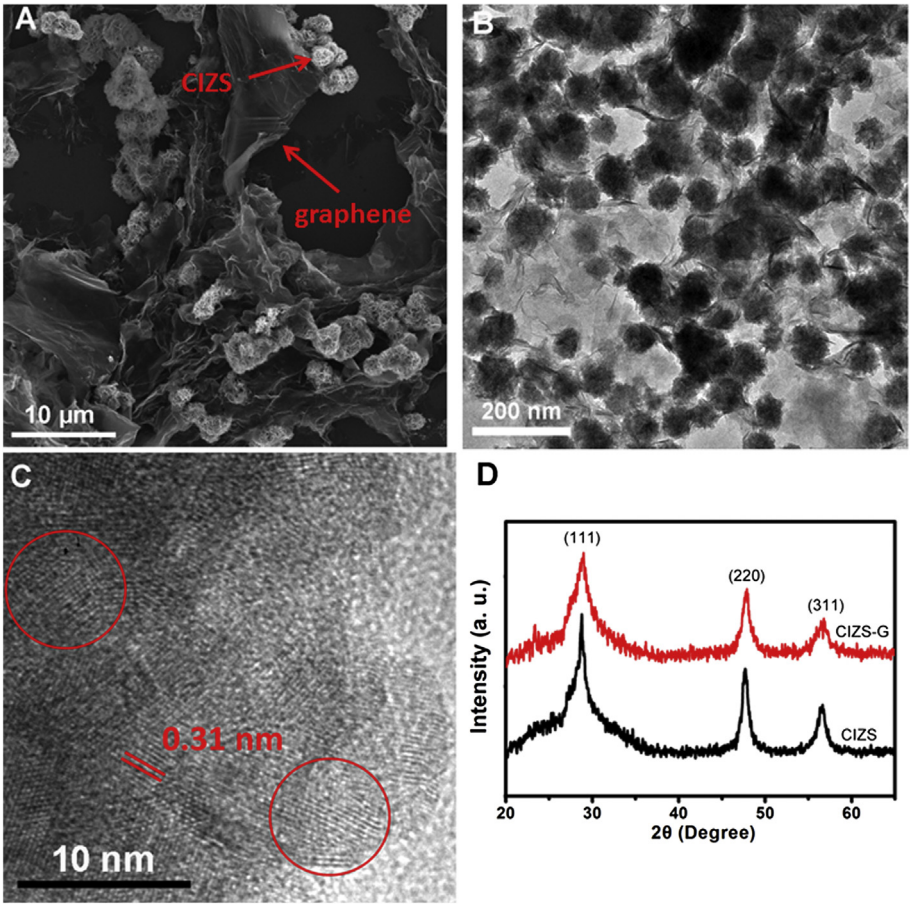

Fig. 1. A) A FESEM image of CIZS@graphene (the weight ratio of graphene/CIZS is 5:95); B) a TEM image of CIZS@graphene; (C) a high-resolution TEM image of CIZS@graphene; D) XRD patterns of the neat CIZS nanospheres and CIZS@graphene.

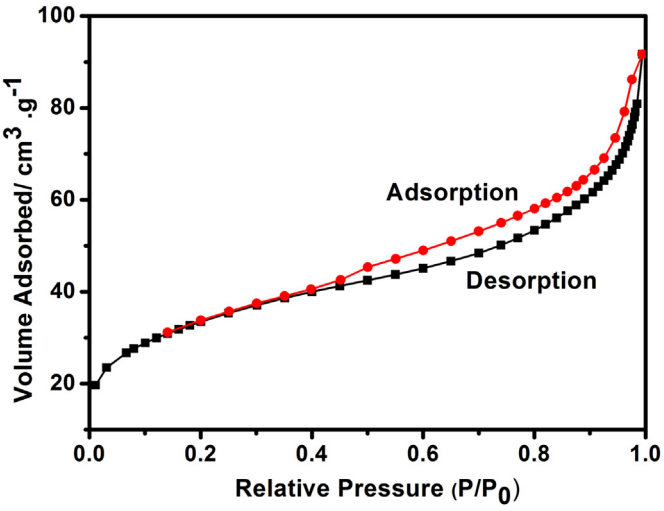

Fig. 2. Nitrogen adsorption–desorption isotherms of the as-prepared CIZS@graphene.

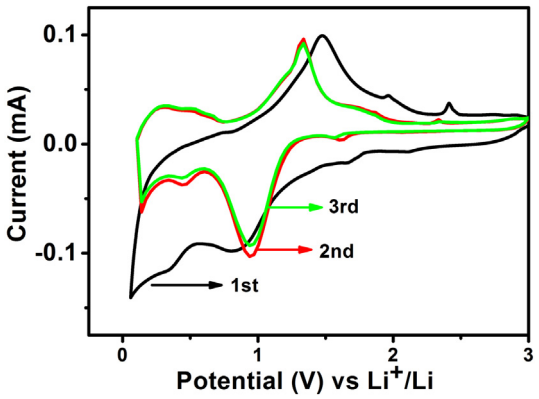

Fig. 4. Cyclic voltammetry of CIZS@graphene in the first three cycles.

type cell with Li metal as the counter electrode (see Experiment section for details). The cell was firstly cycled at 100 mA g^{-1} for three cycles. The corresponding charge–discharge profiles are shown in Fig. 3. In the first discharge curve, an obvious voltage plateau at around 1.1 V versus Li^+/Li^0 can be observed for the anode consisting of the neat CIZS nanospheres (Fig. 3A). The discharge and charge capacities for such an anode are 1213 and 660 mAh g^{-1}, respectively. With CIZS@graphene, the discharge and charge capacities are improved drastically to 1619 mA h g^{-1} and 1060 mAh g^{-1} (Fig. 3B). The initial charge capacity is significantly higher than that of other quaternary or tertiary semiconductor sulfides reported in the literatures. Although the content of graphene is fairly small (5 wt%), it is believed that the graphene

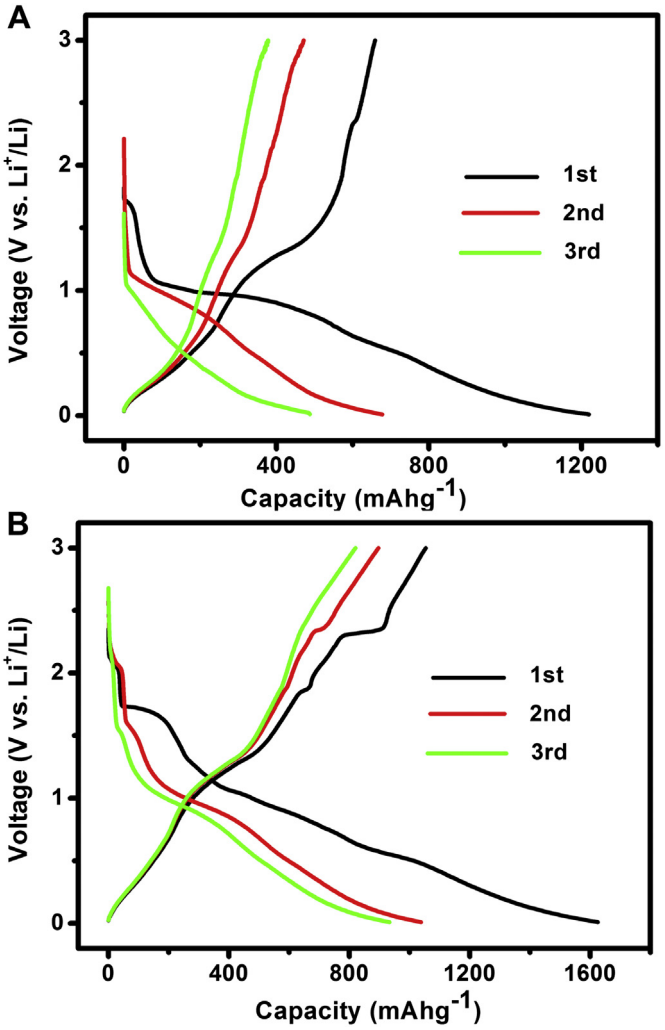

Fig. 3. Charge–discharge profiles of the anodes with CIZS nanospheres (A) and CIZS@graphene (B) as the active material, respectively. The profiles show the first three cycles at a current density of 100 mA g^{-1}.

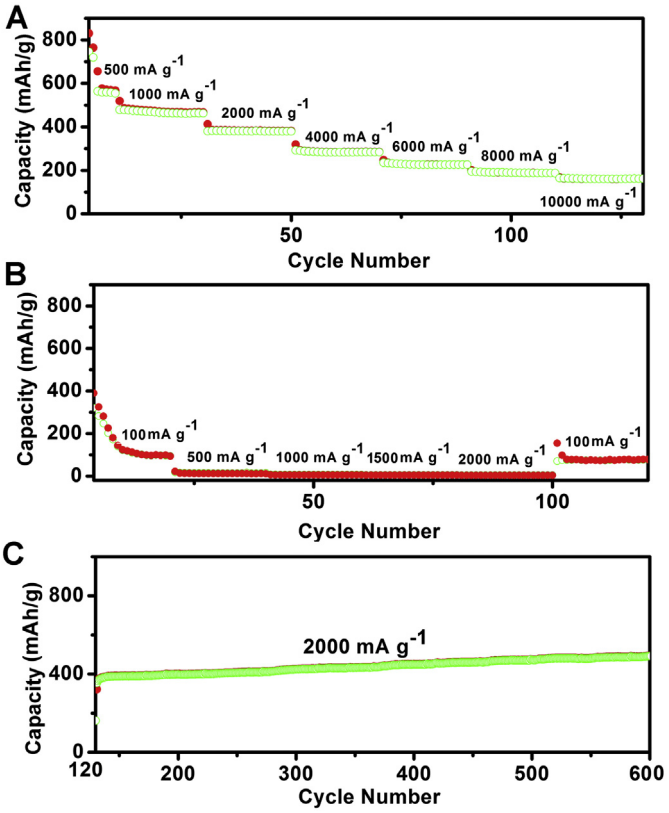

Fig. 5. Capacities of (A) CIZS@graphene and (B) CIZS nanosphere anodes at different current rates; (C) capacities of the CIZS@graphene anode in subsequent cycles.

nanosheets in the anode plays a major role in facilitating electron transport and hence increasing the capacity. The initial capacity loss in the first few cycles might be attributed to the formation of the solid electrolyte interface and the partial pulverization of the CIZS@graphene [24].

To investigate the lithium storage properties of CIZS@graphene, cyclic voltammetry (CV) was performed to probe the corresponding redox reactions. As shown in Fig. 4, in the first cathodic scan, four reduction peaks at 2.12, 1.67, 0.82 and 0.33 V could be observed, which could be attributed to the formation of solid electrolyte interphase (SEI) and the multi-step reduction of the Cu, In, Zn ions [16,17,28]. In the first anodic scan, the obvious oxidation peaks at 1.5 V and above are likely to be caused by the oxidation of Zn and Cu species. In the second cycle, the broad anodic peaks at 0.48 and 0.67 V could be ascribed to the multi-step oxidation of In [16], while the peak at 1.3 V and the plateau at 1.7 V are caused by oxidation of Zn species (they are shifted to lower potentials in comparison with that in the first cycle) [12,17]. The weakening of the peaks implies an irreversible capacity loss in the initial lithiation/delithiation process, which could be ascribed to the formation of SEI layer and the partial pulverization of the CIZS@graphene. The very weak peak at around 2.33 V can be assigned to the oxidation reaction of Cu [17,29]. The CV curves in the third cycle almost replicate that in the second cycle, indicating the reactions are reversible. Although the details of the redox reactions of this new anode material need to be further verified, the above results demonstrate that CIZS indeed has multiple alloying reactions with lithium ions. Based on the previously reported reactions for the related ternary sulfides [14,17] and the CV results presented above, we propose that the capacity of CIZS is mainly contributed by the following three reactions:

$$Cu_{0.02}In_{0.3}ZnS_{1.47} + 2.94Li^+ + 2.94e^- \leftrightarrow 0.02Cu + 0.3In + Zn + 1.47Li_2S \quad c_w = 533\ mA\ h\ g^{-1}$$

$$Zn + xLi^+ + xe^- \leftrightarrow Li_xZn (0 \le x \le 1.5) \quad c_w = 271\ mA\ h\ g^{-1}$$

$$In + xLi^+ + xe^- \leftrightarrow Li_xIn (0 \le x \le 4.33) \quad c_w = 235\ mA\ h\ g^{-1}$$

where c_w represents the incremental contribution to the theoretical capacity by each reaction. The sum of the three c_w values gives CIZS a theoretical capacity value of 1039 mA h g^{-1}.

To further demonstrate the electrochemical performance of the CIZS@graphene nanocomposite electrode, its rate capability was tested and the results are presented in Fig. 5A. The cell was subjected to electrochemical test between 3.0 and 0.05 V under different rates of 500, 1000, 2000, 4000, 6000, 8000 and 10,000 mA g^{-1} with a total cycle number of 125 (5, 20, 20, 20, 20, 20 and 20 cycles for the aforementioned rates, respectively). The first reversible capacities are 563, 505, 389, 313, 248, 202, and 167 mA h g^{-1} at 500, 1000, 2000, 4000, 6000, 8000 and 10,000 mA g^{-1}, respectively. As a comparison, the rate capabilities of the CIZS nanosphere anode was also tested under the same conditions and the results are shown in Fig. 5B. It can be seen that the reversible capacity of the CIZS nanosphere anode quickly fades to around 100 mA h g^{-1} at the current density of 100 mA g^{-1}, and stays at around 10 mA h g^{-1} at the subsequent higher current densities. Compared with the neat CIZS nanospheres, CIZS@graphene exhibits much enhanced rate performance. Specifically, CIZS@graphene could deliver a stable capacity of 563 mA h g^{-1} after 5 cycles at 500 mA g^{-1}, whereas the reversible capacity of the CIZS nanospheres is 64 mA h g^{-1}, which is only ten percent of the reversible capacity of the nanocomposite. At the subsequent current densities, the reversible capacities of CIZS@graphene could reach 167 mA h g^{-1} at an extremely high current density of 10,000 mA g^{-1} after 20 cycles, while the capacity of the CIZS electrode drops drastically to near zero.

The superior cycling performance of CIZS@graphene is further demonstrated in Fig. 5C. It is striking to see that with the current density maintained at 2000 mA g^{-1}, the reversible capacity of the nanocomposite is steadily increased from 389 to 494 mA h g^{-1} after 480 cycles, demonstrating an extremely promising stable cycling performance over a prolonged testing period. The TEM images of CIZS@graphene electrode after cycling for 10 cycles under 2000 mA g^{-1} was showed in Fig. S4, it demonstrated the good structure stability of the as-prepared nanocomposite. When the current density is maintained at 500 mA g^{-1}, the reversible capacity of the nanocomposite is increased from 638 mA h g^{-1} to 900 mA h g^{-1} after 90 cycles (Fig. S5). Such phenomenon can be ascribed to the reversible formation of the gel-like polymeric film on the surface of graphene [24,28,29].

In order to gain insight into the excellent rate performance of the two electrodes, EIS studies were carried out to verify the conductivity-boosting effect of graphene. Fig. 6 shows Nyquist plots of the neat CIZS nanospheres and CIZS@graphene before and after cycling. As demonstrated in Fig. 6A, the diameter of the semicircle for the CIZS@graphene is much smaller than that of the neat CIZS nanospheres, suggesting that the CIZS@graphene anode possesses much lower charge-transfer resistances that lead to its higher initial and cycle capacity [29,30]. The phenomena for increment

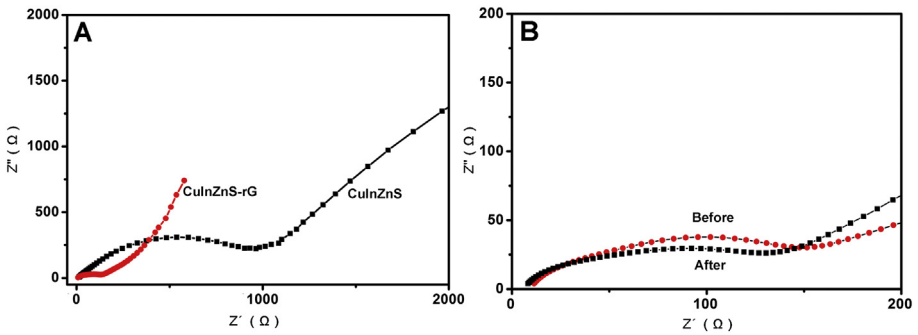

Fig. 6. Electrochemical impedance spectra of (A) the CIZS nanosphere and CIZS@graphene anodes before cycling, and (B) the CIZS@graphene anode before and after cycling.

capacity are often observed in anode or cathode materials, which is generally related to an activation process [31,32]. The activation process is attributed to the fully contact between the active materials and electrolyte upon charge and discharge. Fig. 6B shows the result of the conductivity for CIZS@graphene anode before and after cycling for 480 cycles. It could be observed the interfacial resistance and charge transfer resistance reduced, which gives the evidence for the increment capacity of CuInZnS@graphene under high-rate cycling [26,33–35].

4. Conclusions

In summary, excellent lithium storage performance of CIZS@-graphene has been demonstrated. CIZS is a novel anode material that can have multiple reversible alloying reactions with lithium ions. By synergetic combination of CIZS with highly conductive graphene, the CIZS@graphene anode exhibits an initial discharge capacity of 1623 mA h g^{-1} at 100 mA g^{-1}, and at a high current density of 2000 mA g^{-1} its reversible capacity is steadily increased from 389 mA h g^{-1} to 494 mA h g^{-1} over 480 cycles, demonstrating its outstanding cycling stability at high rates. Such significantly improved high-rate capacity and stability show great promise of this novel nanomaterial for lithium battery applications.

Appendix A. Supplementary data

Supplementary data related to this article can be found at http://dx.doi.org/10.1016/j.jpowsour.2014.01.107.

References

[1] X.W. Lou, Y. Wang, C.L. Yuan, J.K. Lee, L.A. Archer, Adv. Mater. 18 (2006) 2325–2329.
[2] M.S. Park, G.X. Wang, Y.M. Kang, D. Wexler, S.X. Dou, H.K. Liu, Angew. Chem. Int. Ed. 46 (2007) 750–753.
[3] D. Deng, J.Y. Lee, Chem. Mater. 20 (2008) 1841–1846.
[4] M. Armand, J.M. Tarascon, Nature 451 (2008) 652–657.
[5] J.M. Tarason, M. Armand, Nature 414 (2001) 359–367.
[6] Z.S. Wen, D. Lu, J. Electrochem. Soc. 160 (2013) A2311–A2314.
[7] Z.S. Wen, J. Stark, R. Saha, J. Parker, P.A. Kohl, J. Phys. Chem. C 117 (2013) 8604–8610.
[8] K.S. Kang, Y.S. Meng, J. Breger, C.P. Grey, G. Ceder, Science 311 (2006) 977–980.
[9] J.B. Goodenough, Y. Kim, Chem. Mater. 22 (2010) 587–603.
[10] Y. Chen, H. Xia, L. Lu, J.M. Xue, J. Mater. Chem. 22 (2012) 5006–5012.
[11] J.S. Chung, H.J. Sohn, J. Power Sources 108 (2002) 226–231.
[12] L. He, X.Z. Liao, K. Yang, Y.S. He, W. Wen, Z.F. Ma, Electrochim. Acta 56 (2011) 1213–1218.
[13] J.W. Choi, G. Cheruvally, H.J. Ahn, K.W. Kim, J.H. Ahn, J. Power Sources 163 (2006) 158–165.
[14] F.M. Ye, C. Wang, G.H. Du, X.B. Chen, Y.J. Zhong, J.Z. Jiang, J. Mater. Chem. 21 (2011) 17063–17065.
[15] L. Liu, H.J. Liu, H.Z. Kou, Y.Q. Wang, Z. Zhou, M.M. Ren, M. Ge, X.W. He, Cryst. Growth Des. 9 (2009) 113–117.
[16] F.M. Ye, G.H. Du, Z.F. Jiang, Y.J. Zhong, X.D. Wang, Q.P. Cao, J.Z. Jiang, Nanoscale 4 (2012) 7354–7357.
[17] X.S. Yin, C.H. Tang, M.H. Chen, S. Adams, H. Wang, H. Gong, J. Mater. Chem. A 1 (2013) 7927–7932.
[18] B.H. Qu, H.X. Li, M. Zhang, L. Mei, L.B. Chen, Y.G. Wang, Q.H. Li, T.H. Wang, Nanoscale 3 (2011) 4389–4393.
[19] X.S. Tang, Q.L. Tay, Z. Chen, Y. Chen, G.K.L. Goh, J.M. Xue, New J. Chem. 37 (2013) 1878–1882.
[20] A. Jain, G. Hautier, C.J. Moore, S.P. Ong, C.C. Fischer, T. Mueller, K.A. Persson, G. Ceder, Comput. Mater. Sci. 50 (2011) 2295–2310.
[21] Y.X. Li, G. Chen, Q. Wang, X. Wang, A.K. Zhou, Z.Y. Shen, Adv. Funct. Mater. 20 (2010) 3390–3398.
[22] X.S. Tang, Q.L. Tay, Z. Chen, Y. Chen, G.K.L. Goh, J.M. Xue, J. Mater. Chem. A 1 (2013) 6359–6365.
[23] W.F. Chen, S.R. Li, C.H. Chen, L.F. Yan, Adv. Mater. 23 (2011) 5679–5683.
[24] Y. Chen, B.H. Song, X.S. Tang, L. Lu, J.M. Xue, J. Mater. Chem. 22 (2012) 17656–17662.
[25] S.Q. Chen, Y. Wang, J. Mater. Chem. 20 (2010) 9735–9739.
[26] Z.S. Wu, W.C. Ren, D.W. Wang, F. Li, B.L. Liu, H.M. Cheng, ACS Nano 4 (2010) 5835–5842.
[27] X.G. Mei, J.Y. Ouyang, Carbon 49 (2011) 5389–5397.
[28] J.H. Kong, Z.L. Liu, Z.C. Yang, H.R. Tan, S.X. Xiong, S.Y. Wong, X. Li, X.H. Lu, Nanoscale 4 (2012) 525–530.
[29] W.H. Zhou, Y.L. Zhou, J. Feng, J.W. Zhang, S.X. Wu, X.C. Guo, X. Cao, Chem. Phys. Lett. 546 (2012) 115–119.
[30] G.M. Zhou, D.W. Wang, F. Li, L.L. Zhang, N. Li, Z.S. Wu, L. Wen, G.Q. Lu, H.M. Cheng, Chem. Mater. 22 (2010) 5306–5313.
[31] Y. Zhao, J.X. Li, N. Wang, C.X. Wu, Y.H. Ding, L.H. Guan, J. Mater. Chem. 22 (2012) 18797–18800.
[32] L. Qie, W.M. Chen, Z.H. Wang, Q.G. Shao, X. Li, L.X. Yuan, X.L. Hu, W.X. Zhang, Y.H. Huang, Adv. Mater. 24 (2012) 2047–2050.
[33] J. Yang, Q.C. Liao, X.Y. Zhou, X.J. Liu, J.J. Tang, RSC Adv. 3 (2013) 16449–16455.
[34] H.Q. Cao, B.J. Li, J.X. Zhang, F. Lian, X.H. Kong, M.Z. Qu, J. Mater. Chem. 22 (2012) 9759–9766.
[35] S. Laruelle, S. Grugeon, P. Poizot, M. Dolle, L. Dupont, J.M. Tarascon, J. Electrochem. Soc. 149 (2002) A627–A634.